Bulletin of the Seismological Society of America, Vol. 88, No. 1, pp. 304–312, February 1998

# Pseudo Green's Functions and Waveform Tomography

by Xi J. Song and Donald V. Helmberger

Abstract Retrieving source characteristics for moderate-sized earthquakes in sparsely instrumented regions has been made possible in recent years, through the modeling of waveforms at regional distances. The techniques used in such studies model waveforms successfully at long period, using Green's functions for simple 1D crustal models. For small earthquakes ($M < 4$), however, long-period signals are usually noisy, and modeling short-period waveforms requires refined Green's functions such as used in the empirical Green's function (eGf) approach. In this article, we present a new technique that generates such Green's functions by perturbing individual generalized ray responses calculated from a 1D model. The model is divided into blocks, and velocities in the blocks are allowed to vary, which shifts the arrival time of the individual rays similar to conventional tomography. The amplitudes of the rays are perturbed independently to accommodate local velocity variations in the structure. For moderate-sized earthquakes with known source mechanism and time history, the velocity variation in each block and the amplification factor for individual rays can be optimized using a simulated annealing algorithm. The resulting modified Green's functions, pseudo Green's functions (pGfs), can be used to study the relative location and characteristics of neighboring events. The method is also useful in retrieving 2D structure, which is essentially waveform tomography.

## Introduction

Many earthquakes have occurred in southern California since the introduction of the TERRAscope array. Nearly 400 events have been recorded broadband with magnitude greater than 3.5. Techniques for inverting long-period data to obtain first-order source parameters such as mechanism, depth, and moment have become well developed, for example, Dreger and Helmberger (1991), Ritsema and Lay (1995), Zhu and Helmberger (1996). These techniques model waveforms successfully at long period, using Green's functions for simple 1D crustal models. Currently, these efforts are limited to earthquakes with magnitude greater than 4.0. The nature of the difficulty can be seen by comparing the recordings of a typical earthquake sequence of different magnitude. Figure 1 displays broadband and long-period records of the 1991 Sierra Madre earthquake and two of its aftershocks (Fig. 2). As can be seen, long-period noise tends to overwhelm the signal at about magnitude 3.5. To study small events, it is necessary to avoid long-period signals in the broadband recordings and model shorter-period waveforms. Doing this requires refined Green's functions.

One of the applications, or usefulness, of point-source parameters is to fine-tune the propagation model involved and further investigate structure heterogeneity. The method of Zhao and Helmberger (1994), further improved by Zhu and Helmberger (1996), is a natural approach toward this goal. This method matches observed seismograms against synthetics over discrete wave trains and allows relative time shifts between individual wave trains, for example, the $P_{nl}$ wave train and the Rayleigh wave (hence the name "cut and paste"). This allows a better correlation between data and synthetic waveforms. One example of this method as applied to the 28 June, 17:00, 1991 Sierra Madre aftershock (Fig. 2) is shown in Figure 3. The upper panel shows the source inversion using long-period records from stations GSC, PFO, and ISA. Synthetics at station SBC are predictions with the resulting source mechanism. The lower panel displays the predicted broadband synthetics at all four stations. The waveforms are well matched, especially the long-period records at stations GSC, PFO, and ISA. The *SV* waves are used together with the Rayleigh waves, and the latter dominates the comparison between the data and synthetics, as seen in the complete radial and vertical components (Fig. 3). However, it seems that a small timing perturbation would bring the *SV* synthetics into alignment with the observation (e.g., station ISA). This is more clearly seen on the vertical components (Fig. 3, lower panel). These time shifts, together with those for the $P_{nl}$ waves, the Love waves, and the Rayleigh waves, are indicative of further adjustment of model velocities, as discussed in Song *et al.* (1996). However, all these time shifts may not be satisfied with adjustments to a 1D model. Furthermore, timing perturbations on individual arrivals would fit the data to a higher level of detail and

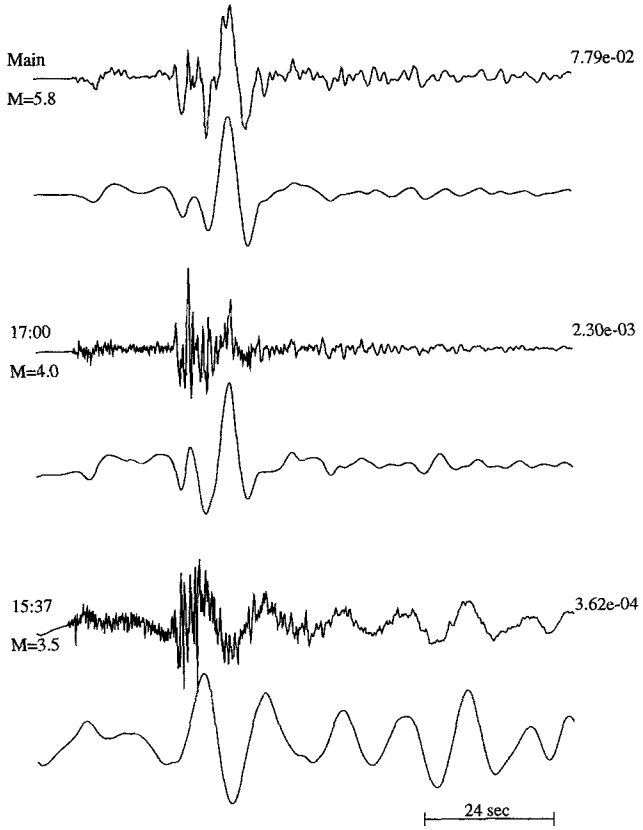


Figure 1. Comparison of broad and long-period data for the 1991 Sierra Madre sequence. The top pair of traces show the recording at station GSC for the 1991 Sierra Madre mainshock, with the upper trace broadband and the lower trace filtered with a long-period Press–Ewing instrument response. The next two pairs display the comparison for two aftershocks.

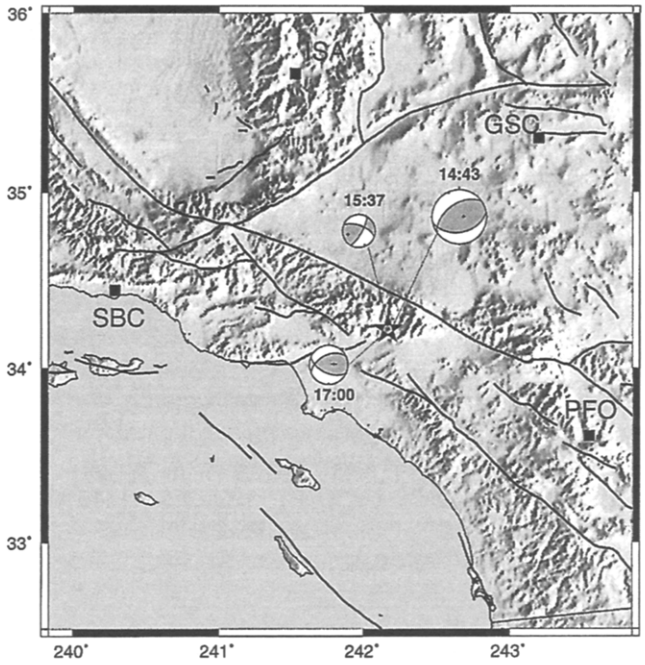


Figure 2. Topographic map of southern California and epicenters and source mechanisms of the Sierra Madre mainshock and its two aftershocks. Also shown are the locations of four TERRAscope stations used in this study.

would even fix the problems for station SBC (Fig. 3). One immediate question that follows such observations is how to adjust the velocity structure to achieve these fine timing perturbations. Or, if this question turns out to be too difficult to answer for some cases, is it possible, from a practical point of view, to perform such perturbation and make use of the resulting high-resolution Green's functions? This article tackles these questions.

High-resolution Green's functions are useful and necessary to study the initiation process and source complexity of large events. For these purposes, we have resorted to empirical Green's functions (eGfs) (Hartzell, 1978). However, the application of eGfs is limited by many factors, such as source mechanism and location. Thus, our success in recovering higher-order parameters such as rupture properties have been limited, largely due to the inability to correct for propagational effects at short periods. In other words, we have not been able to exploit the broadbandness of the TERRAscope data routinely because of the lack of quality broadband Green's functions.

In this article, we present a new technique that generates such Green's functions, or pseudo Green's functions (pGf) as we call them. Pseudo Green's functions are less dependent on source mechanism and can be adjusted for small difference in source location. The technique is tested on the Sierra Madre earthquake of 28 June 1991 and its two aftershocks on the same day (Fig. 2). The pGfs obtained from the $M_L$ = 4.0 aftershock at 17:00 GMT are used to model a smaller aftershock of $M_L$ = 3.5 at 15:37 GMT. These events are chosen because they occurred in the middle of the TERRAscope array and occurred within 2 km of each other (Hauksson, 1994). Previous studies (e.g., Dreger and Helmberger, 1991; Zhao and Helmberger, 1994; Hauksson, 1994) provide essential information needed in our experiments, for example, source location, depth, mechanism, and source-time function. Application of the pGf technique in waveform tomography is also discussed.

## From eGf to pGf—The pGf Method

From the generalized ray theory (Helmberger, 1983), a synthetic seismogram consists of a series of ray responses that describe energy packets arriving at the receiver along various paths. The travel time of an individual ray is controlled by the integral slowness along its path. A mild perturbation of the 1D model usually preserves the shape of the ray responses (Song *et al.*, 1996). This is demonstrated in Stead (1990), where he conducted finite-difference computation of a set of similar 2D models. The amplitudes of the

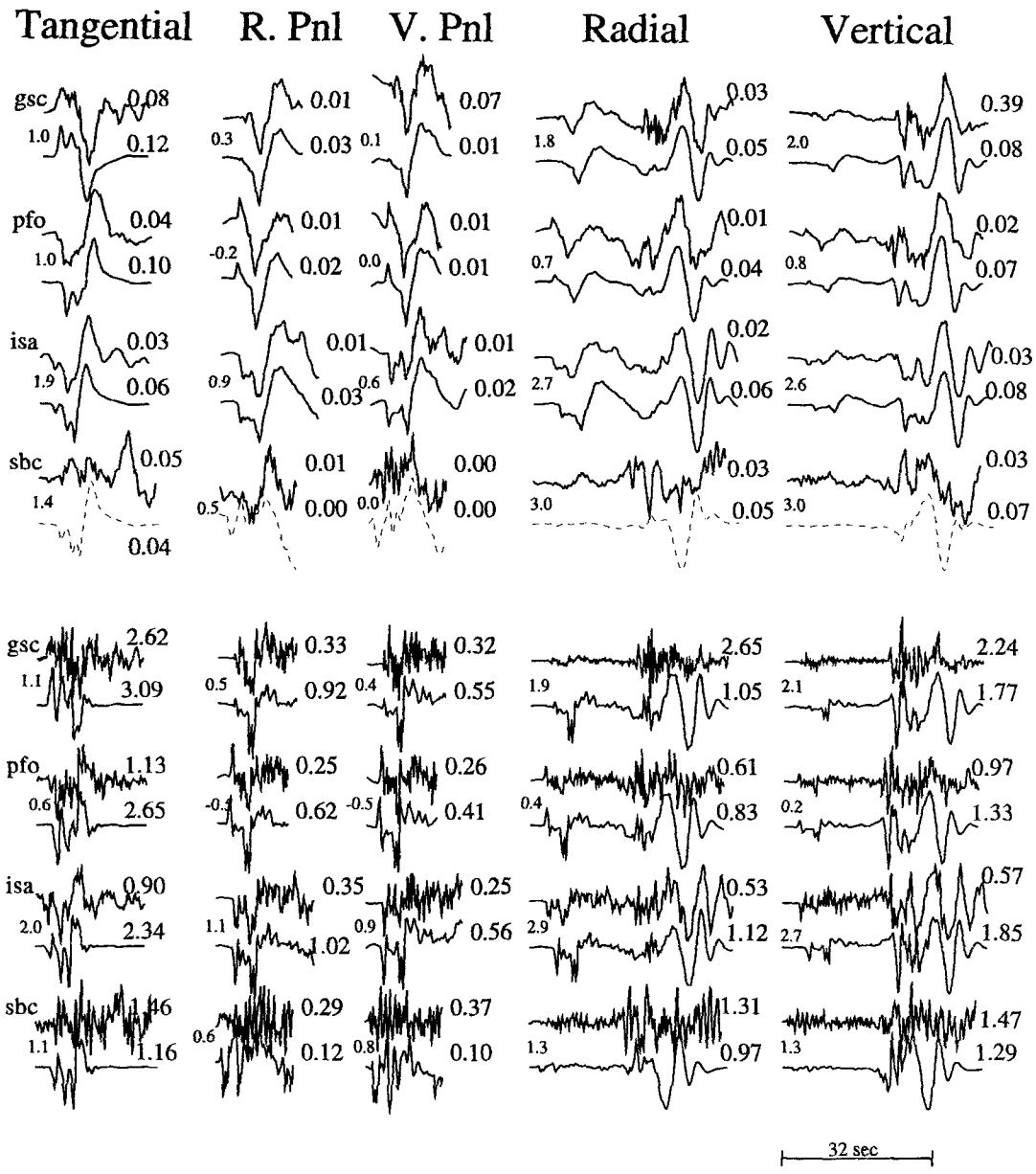


Figure 3. Comparison of data and SC synthetics for the Sierra Madre aftershock (17:00). The upper panel shows the result of the source estimation process with stations GSC, ISA, and PFO. A source mechanism of (244°, 48°, 51°) is obtained, with a source-time function of (0.2, 0.3, 0.2 sec). The $P_{nl}$ waves are enlarged and shown separately, as they are processed in the inversion routine. Synthetics at station SBC are predictions. The lower panel shows broadband predictions of the SC synthetics with the source mechanism derived from the long-period data (upper panel). Peak amplitudes are shown at the end of each trace. Small numbers indicate time delay of synthetics relative to data. After Zhao and Helmberger (1994).

ray responses, however, are more sensitive to the velocity perturbation and usually depend on very local changes in the model.

The method we describe in this section resembles the conventional travel-time tomography in that travel times of individual rays are connected to a slowness model, which consists of discrete, constant slowness cells. Besides modeling the travel time of the first arrival, all important pulses on a seismogram are taken into consideration. These travel times ($t_0$'s of the generalized rays) are fit by matching the waveform data with the total synthetics [$S(t)$], which is the sum of all the individual ray responses [$R(t)$], after being shifted by $dt$ and amplified by a factor $A$:

$$S(t) = \sum_i A_i R_i(t) * \delta(t - dt_i), \qquad (1)$$

where $i$ is the index to the rays and * denotes time-domain convolution. Convolution with the $\delta$ function in (1) corresponds to a time shift. The ray response $R_i(t)$ is computed from a reference 1D model. The time shift $dt_i$ is formulated as in conventional travel-time tomography:

$$dt_i = \sum_j l_{ij} ds_j, \tag{2}$$

where $ds_j$ is the velocity perturbation to block $j$ and $l_{ij}$ is the length for which ray $i$ travels in block $j$. To minimize the effect of the amplitudes of the ray responses on fitting the travel time, $A_i$'s are allowed to change freely over a restricted range. This freedom in the parameterization also serves to obtain practical Green's functions, or the pGfs, as is discussed later.

Unlike the conventional travel-time tomography that usually features linearized inversion, our pGf technique takes a forward approach. A set of optimal parameters, the slowness perturbation in the model blocks ($ds_j$) and the amplification factor ($A_i$) for individual rays, are determined using a simulated annealing algorithm. Simulated annealing algorithms have become widely used in recent seismological studies (e.g., Sen and Stoffa, 1991; Ammon and Vidale, 1993; Zhao and Frohlich, 1996). Among these, Zhao and Frohlich (1996) described a modification and optimization of the algorithm, which is employed in our exercise. While Zhao and Frohlich (1996) used both the L1 and L2 norms between data and synthetics in their objective function, we use the L2 norm alone for practical reasons. The L2 norm between a synthetic described by equations (1) and (2) and the corresponding data can be computed with little expense, using fast Fourier transform (Song *et al.*, 1997). The evaluation of the L1 norm, however, is quite expansive in our situation. Thus, excluding the L1 norm allows sufficiently low cooling rates that in turn enhances the chance of finding the global minimum. After a set of optimal parameters ($ds_j$, $A_i$) is found, the time shifts of the rays ($dt_i$) are computed again from the optimal velocity perturbation ($ds_j$) with equation (2). These optimal time shifts, together with the optimal amplification factors ($A_i$), are applied to the original 1D impulse ray responses to generate the pGfs for the fundamental fault system, which consists of strike-slip, dip-slip (90° dip), and 45° dip-slip orientations.

Figure 4 shows an example of the pGf technique as applied to the 1991 Sierra Madre mainshock and the big aftershock (17:00). In this experiment, the standard southern California model of Dreger and Helmberger (1991) is used as the reference model (Table 1). Green's functions are combined with the source mechanism, source-time function, and seismic moment of Zhao and Helmberger (1994) for both events to generate the original 1D ray responses. In this figure, individual ray paths and responses are shown only for the most important rays, while the total synthetics contain a total of 14 rays. These rays comprises a sufficient ray set to match the complete synthetics as generated by the reflectivity method (Saikia, 1994). All seismograms are plotted in absolute time with the same amplitude scale. In column (a), each layer of the original 1D model (SC) is perturbed as a single block. This setup has the minimal freedom in terms of fitting the travel times. As a result, the onset of the simulation, that is, the sum of the rays after shifting and amplification, is slightly off, as compared to the data. The overall waveform, however, is well matched. If we take the resulting model, shown at the bottom, and compute 1D synthetics for it, the new synthetics would be the dotted trace shown superimposed on the perturbation result in the lower panel. This comparison of the two synthetics demonstrates the goodness of the time-shift approximation. The strength of the pulses on these two synthetics does not match exactly, and we picture the amplification effect as a result of many other factors, including source complexity and very local variation in the model, which we do not intend to model in this example. Column (b) displays another test on the aftershock. This time, the SC model is divided into 10 blocks, the slowness of which can vary independently. As a result of more freedom, the resulting simulation match the data better than in column (a). In Column (c), the same experiment is conducted using the mainshock data recorded at station GSC. As can be seen in the comparison of columns (b) and (c), the time shifts for most of the rays are consistent for the two events. However, the corresponding slowness models show a substantial difference. This brings up the nonuniqueness problem in the process of producing the required travel-time shifts.

In Figure 5, a set of experiments, showing a spectrum of parameterization schemes, is displayed. In general, as the starting model is divided into more blocks, the waveform fit is improved, but the corresponding models for different events show greater difference. The dotted traces show a case where the time shifts of the individual rays are not connected by any physical model. The simulations fit the data almost exactly, but there is no way of transporting the optimal parameters from event to event. In the rest of our experiment, we choose to divide the model into six blocks since this setup seems to generate reasonable synthetic fits as well as model stability.

## Application to the Sierra Madre Aftershocks

We applied the above procedure to paths from Sierra Madre to stations GSC, ISA, PFO, and SBC, using the tangential component of the broadband displacement data from the big aftershock (17:00). The aftershock data is used instead of the mainshock because presumably it is less contaminated by source complexity. Figure 6 shows the comparison between the data, the simulations, and the original 1D SC synthetics. The simulations fit the data well for all stations, both in wave shape and amplitude. Station SBC shows the most improvement over the original 1D synthetics. All the models display low velocity in regions near the

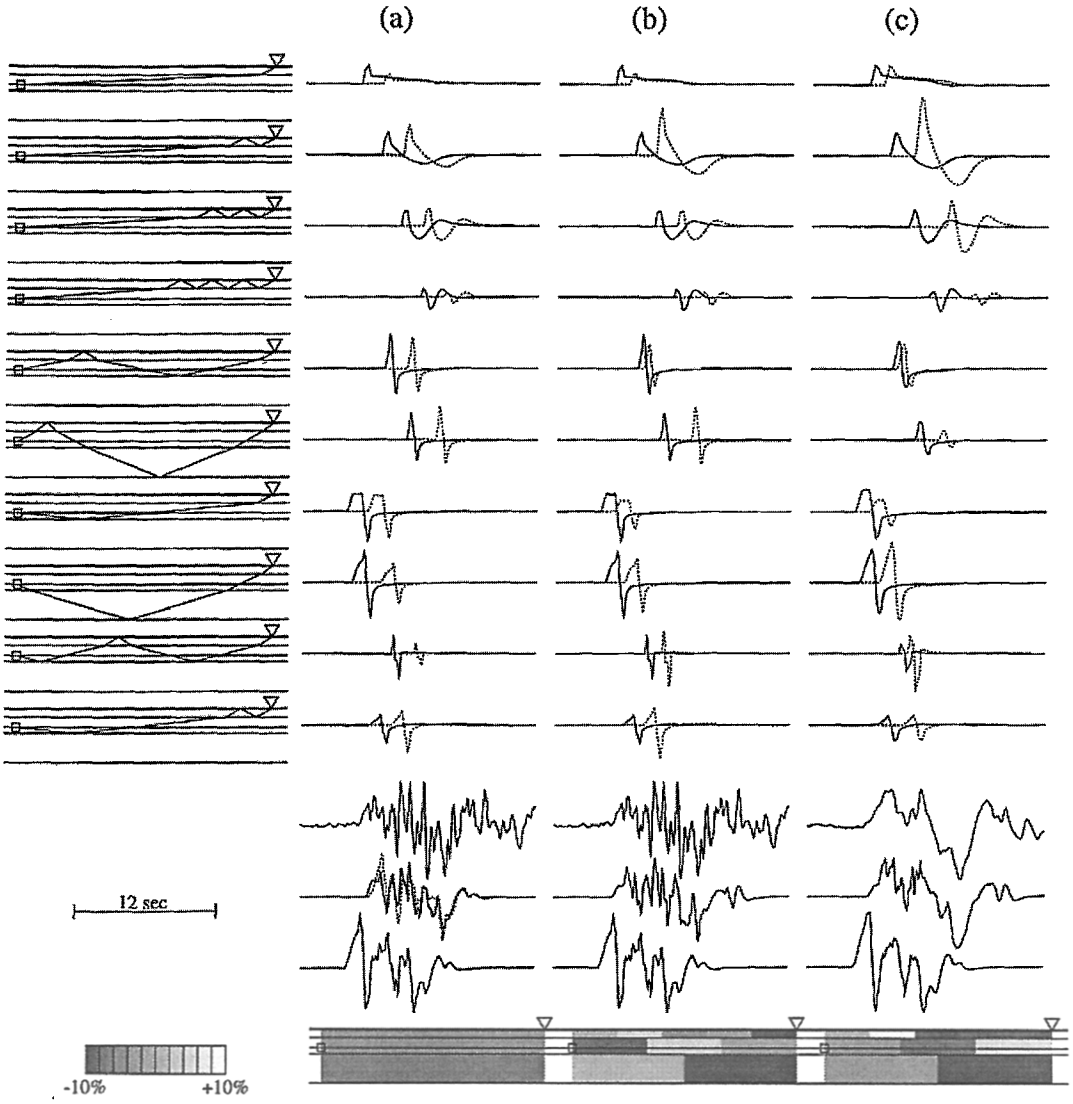


Figure 4. The pGf procedure used in generating pGf for the path from Sierra Madre to station GSC. The leftmost column shows the individual ray paths corresponding to the point-source responses shown to the right. Columns (a) and (b) are for the big aftershock (17:00), and column (c) is for the mainshock (14:43). Note column (a) allows only 1D velocity changes, while in columns (b) and (c), the model is divided into 10 blocks. The lower three sets of seismograms (solid traces) contain the data, the pGf simulation, and the SC synthetic (bottom traces). The dotted trace in the lower panel in column (a) is the new 1D synthetic for the model shown at the bottom of the same column. Point-source solution of Zhao and Helmberger (1996) is used.

Table 1

Model parameters. After Dreger and Helmberger (1991). $Z$ is the depth to the top of the layer.

| $V_p$ (km/sec) | $V_s$ (km/sec) | $\rho$ (g/cc) | $Z^1$ (km) |
|---|---|---|---|
| 5.5 | 3.18 | 2.4 | 0.0 |
| 6.3 | 3.64 | 2.67 | 5.5 |
| 6.7 | 3.87 | 2.8 | 16.0 |
| 7.8 | 4.5 | 3.0 | 35.0 |

source, which could be real or caused by an error in origin time.

Again, if we apply the time shifts ($dt_i$) and amplification factors ($A_i$) found in the foregoing pGf procedure to the original 1D impulse ray responses for the basic faults, we obtain pGfs as shown in Figure 7 for the path from the big aftershock to station SBC. These responses are fine-tuned, that is, shifted in time and amplified, in the previous procedure to suit this particular path.

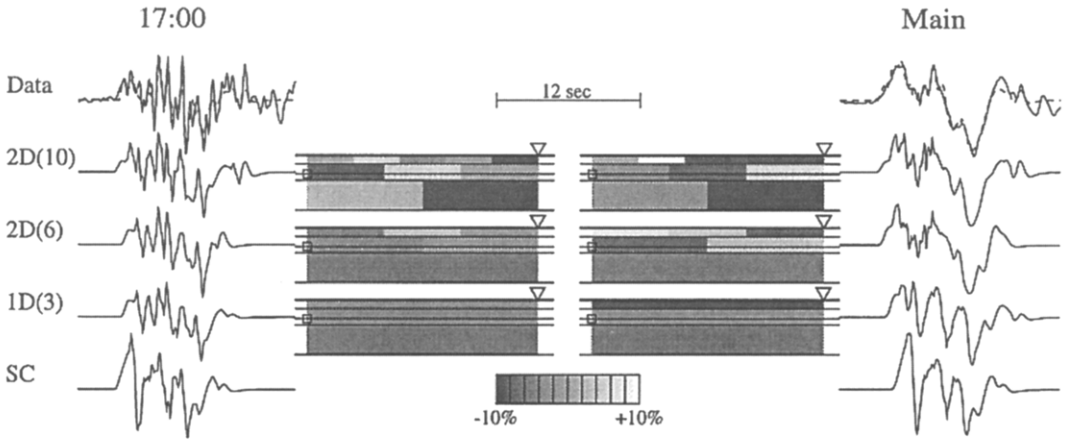


Figure 5. Data and simulations with different schemes of model division in the pGf procedure. Tangential component of broadband displacement data at station GSC is used. The results for the mainshock (right) and those for the aftershock (left) are compared. The original 1D SC synthetics are shown at the bottom.

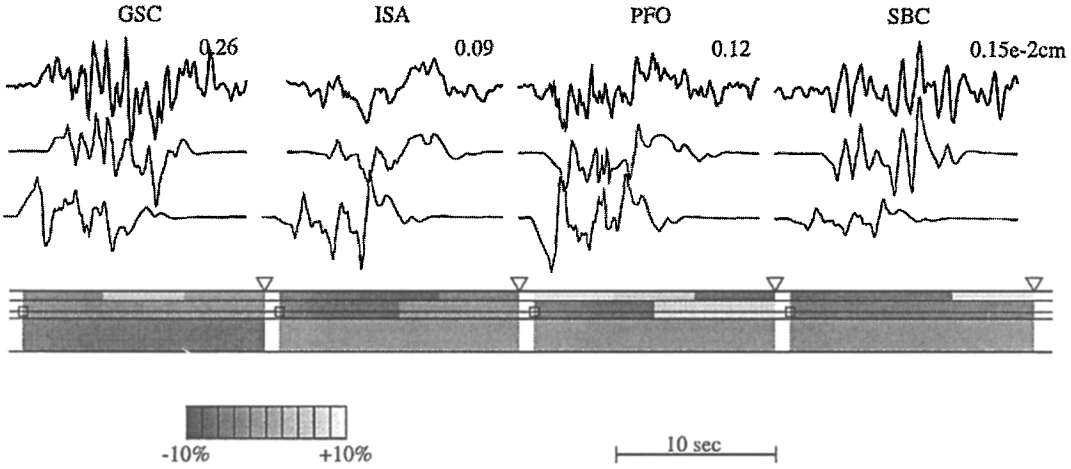


Figure 6. Psuedo Green's function simulations (middle traces) and the associated 2D models from Sierra Madre to four TERRAscope stations. Tangential component of broadband displacement data (top traces) from the big aftershock is used. The SC model is used as the starting model for all paths. The point-source solution of Dreger and Helmberger (1991) is used. The original 1D SC synthetics (bottom trace) are also shown for comparison.

In Figure 5, we have seen some similarities between the models derived for similar paths using the aftershock data and the mainshock data. This suggests similar time shifts are involved for the ray responses in the resulting pGf simulations. One immediate question is how the pGfs derived from one event can be used to model another neighboring event. The most straightforward application that can address this issue is to invert for the source mechanism of a closely located small event with known mechanism. To this end, we choose the small aftershock (15:37) that is located within 2 km of the big one (Hauksson, 1994). Figure 8 shows the source inversion result for this small aftershock (15:37) with the method of Zhao and Helmberger (1994). In this inversion, the tangential component of the broadband displacement data is modeled using the pGfs derived in the above test using data from the big aftershock (17:00). Broadband waveform data for an event of this size ($M_L$ = 3.5) can be difficult to use for inversion of source mechanism if the relative timing between different high-frequency-rich phases (e.g., *sSmS* and *SmS*) in the Green's functions is off, which is the case for the 1D SC synthetics. The pGfs seem to do well in this respect for all four stations, and the source mechanism result agrees with the focal plot (Fig. 2) determined from first-motion *P*-wave picks from the Southern California Seismic Network (SCSN) (Hauksson, 1994). Station SBC is usually problematic when modeling events from the east, due to the complex propagation effect associated with the basins along the path. However, stations in this azimuth are

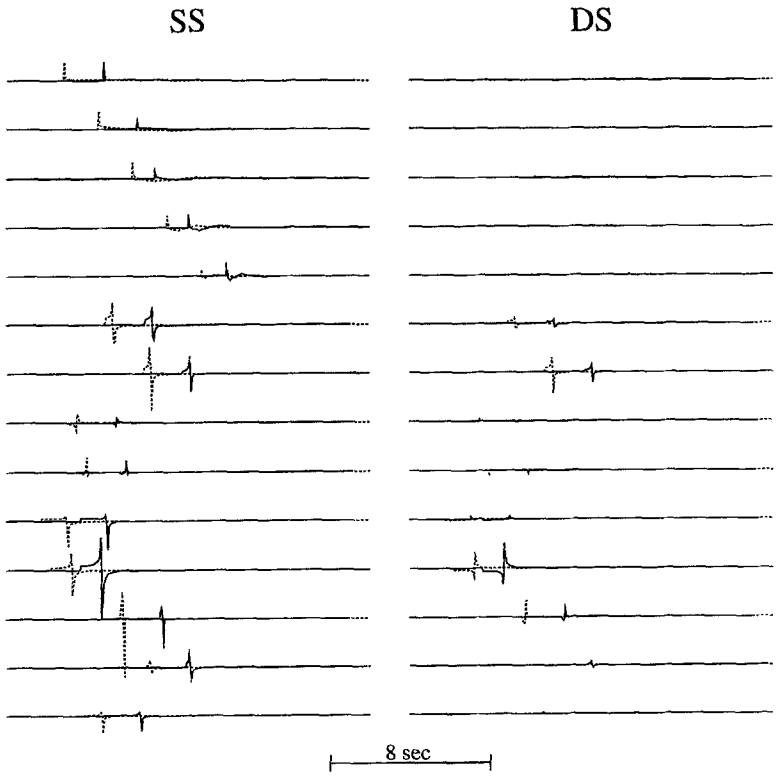


Figure 7. Strike-slip (left) and dip-slip (right) impulse ray responses (solid traces) that form the pGfs from the big aftershock (17:00) of Sierra Madre to station SBC. The dotted traces are the original 1D SC Green's functions.

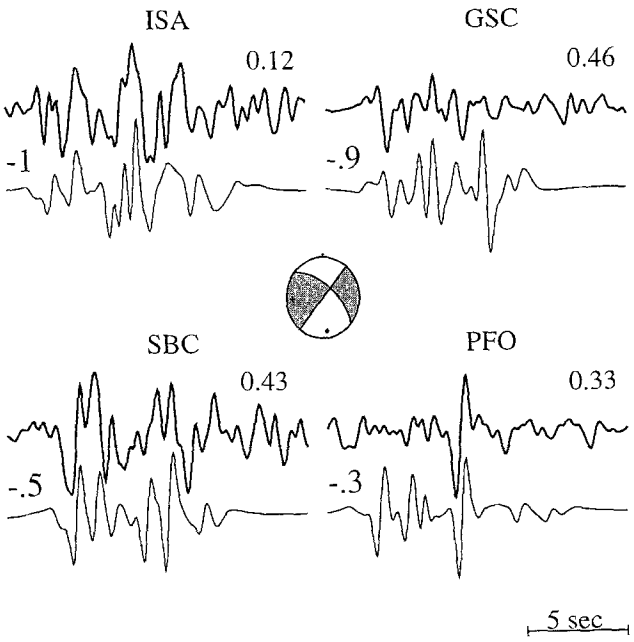


Figure 8. Comparison of the tangential component of the broadband displacement data of the small aftershock (15:37) and the simulations with eGfs derived using data from the big aftershock (17:00) for the same paths. The best-fitting source mechanism, shown at the center, and a source-time function of (0.2, 0.1, 0.2) sec are used to produce the simulations.

critical to the modeling of events in the Los Angeles region because there is already a gap in the distribution of stations to the southwest due to the Pacific ocean. With the pGfs, the waveform fit to station SBC is satisfactory (Fig. 8).

We notice that there are problems in the waveform fit in Figure 8 (e.g., at stations PFO and GSC). The late part of the record at station PFO is fit reasonably well, but there is a problem with the front. For station GSC, however, the phase *sSmS* on the synthetic is too strong when compared to the data. A tentative explanation for this is that the big aftershock occurred on a northeast-dipping thrust fault and probably ruptured upward, which strengthened the *sSmS* arrival from the big aftershock, especially at station GSC. In other words, when the pGfs functions were generated, they already had in them a source directivity that is not in the small aftershock. One remedy to this is to simultaneously invert multiple well-located events and average out the effect of source directivity on the arrival time.

## Discussion and Summary

Our pseudo Green's functions take the form of a set of impulse ray responses to the fundamental faults, as shown in Figure 7. In the Sierra Madre example, we simply summed the impulse responses and used the resulting two-component Green's functions (strike slip and dip slip) in the source in-

version procedure. In reality, if a small aftershock is in the neighborhood of a big aftershock but of some distance away from it, we can further adjust the arrival time of each individual ray response in the pGfs by applying the travel-time perturbation analysis discussed in Song and Helmberger (1996). On the other hand, if we have one well-located small event with a source mechanism known, we can invert for the relative location of a group of neighboring events, using pGfs. Furthermore, if we make the assumption that a large event is a sum of small events, we can study the source finiteness and rupture directivity of large events by accurately locating the relative position and timing of the subevents in a large earthquake.

It appears that the pGf technique could be effective in fine-tuning a 1D model per path, as displayed in Figure 4. To do that, one begins with a starting model and computes the impulse responses of a sufficient set of generalized rays. After an optimal set of velocity variations is found, the ray responses are updated using the resulting model. With this new model as the reference, another iteration can start. Our experiments with 1D models show that this process converges, if given a reasonable starting model. In fact, with recently developed techniques for fast computation of 2D ray synthetics, it is possible to fine-tune a 2D model per path. For example, one can apply the local earth stretching approximation of Helmberger *et al.* (1996) to compute 2D generalized ray responses at regional distances. For larger distances, one can trace the ray paths in a 2D block model, thus modifying the ray parameter–travel-time curve, and conduct a WKM integration to compute synthetic responses associated with a particular path, as discussed in Ding (1997). These two techniques can be easily incorporated into the above-mentioned iteration process for fine-tuning a 2D model.

The amplification factors used to generate the pGfs can offer additional information. Site condition, attenuation, local velocity changes in the model, and source complexities all contribute to the changes of the amplitude of ray responses. Practically, the amplitude factors and the time shifts can be studied separately since many times only one of them is important in the problem. In fact, such separation reduces the number of parameters in the annealing process and effectively speeds up the simulation. In our Sierra Madre test, we have put off the consideration of the contributing sources of the amplification factors, since we were mainly interested in getting usable Green's functions. However, because of the nature of the algorithm we use to find the pGfs, that is, the simulated annealing algorithm, it is possible to represent these factors as a combination of the site response and the source directivity and invert them simultaneously when searching for the pGfs. These amplification factors can also be incorporated into the local earth stretching approximation and associated with the transmission and reflection coefficients in the simulation process.

In this development of a new technique, we have concentrated on the tangential component of the ground motion because of its simplicity as compared to the *P–SV* system. In the future, however, it is possible and necessary to use the full ground motion by employing three-component data. It is also possible to invert multiple events and multiple stations in a single simulation, as discussed in Song *et al.* (1997). Combined with the above-mentioned techniques of generating 2D ray synthetics, it is foreseeable that we would be able to test existing 3D *P*-wave tomographic models with waveform details and develop 3D pictures of *S*-velocity structure.

In summary, we have introduced a new technique to generate highly accurate practical Green's functions for modeling regional phases. The pGfs are constructed with the generalized rays from a 1D reference model, using empirical Green's functions as guidelines. The variations of the arrival times of the rays are connected by perturbations to the velocity model, like the conventional travel-time tomography. The optimal model is found with a simulated annealing algorithm. We have showed that pGfs are useful in studying neighboring events. Our ongoing effort includes further developing this technique for the purpose of waveform tomography and for detailed studies of the source process of large earthquakes.

## Acknowledgments

We thank Dr. Hong Kie Thio and Dr. Eiichi Fukuyama for reviewing the manuscript. This research was supported by the Department of Defense and was monitored by the Air Force, Office of Scientific Research, under Contract Number 64598. It is also supported by SCEC under Contract Number 64527, as funded by NSF #89-20136 and USGS #1434-93-G-2322. Contribution Number 5812, Division of Geological and Planetary Sciences, California Institute of Technology, Pasadena, California.

## References

Ammon, C. J. and J. E. Vidale (1993). Tomography without rays, *Bull. Seism. Soc. Am.* **83,** 509–528.

Ding, X. (1997). High resolution modeling of deep earth structure, *Ph.D. Thesis,* California Institute of Technology, Pasadena, California.

Dreger, D. and D. V. Helmberger (1991). Source parameters of the Sierra Madre earthquake from regional and local body waves, *Geophys. Res. Lett.* **18,** 2015–2018.

Hartzell, S. H. (1978). Earthquake aftershocks as Green's functions, *Geophys. Res. Lett.* **5,** 1–4.

Hauksson, E. (1994). The 1991 Sierra Madre earthquake sequence in southern California: seismological and tectonic analysis, *Bull. Seism. Soc. Am.* **84,** 1058–1074.

Helmberger, D. V. (1983). Theory and application of synthetic seismograms, in *Earthquakes: Observation, Theory and Interpretation,* H. Kanamori (Editor), Soc. Italiana di Fisica, Bologna, Italy, 173–222.

Helmberger, D. V., L.-S. Zhao, and E. Garnero (1996). Construction of synthetics for 2-d structures; core phases, in *Seismic Modeling of Earth Structure,* A. M. Enzo Boschi and Göran Ekström (Editors), Istituto Nazionale di Geofisica, Editrice Compositori, 183–222.

Ritsema, J. and T. Lay (1995). Long-period regional wave moment tensor inversion for earthquakes in the western United States, *J. Geophys. Res.* **100,** no. B7, 9853–9864.

Saikia, C. K. (1994). Modified frequency-wavenumber algorithm for regional seismograms using filon-quadrature method—modeling of $l_g$ waves in eastern North America, *Geophys. J. Int.* **118,** 142–158.

Sen, M. K. and P. L. Stoffa (1991). Nonlinear one-dimensional seismic waveform inversion using simulated annealing, *Geophysics* **56,** 1624–1638.

Song, X. J. and D. V. Helmberger (1996). Source estimation of finite faults from broadband regional networks, *Bull. Seism. Soc. Am.* **86,** 797–804.

Song, X. J., L.-S. Zhao, and D. V. Helmberger (1996). Broadband modeling of regional seismograms; the Basin and Range crustal structure, *Geophys. J. Int.* **125,** 15–29.

Song, X. J., L. Zhu, and D. V. Helmberger (1997). Waveform tomography and crustal structure of the Tibetan plateau, paper in preparation.

Stead, R. (1990). Finite differences and a coupled analytic technique with applications to explosions and earthquakes, *Ph.D. Thesis,* California Institute of Technology, Pasadena, California.

Zhao, L.-S. and C. Frohlich (1996). Teleseismic body-waveforms and receiver structures beneath seismic stations, *Geophys. J. Int.* **124,** 525–549.

Zhao, L.-S. and D. V. Helmberger (1994). Source estimation from broadband regional seismograms, *Bull. Seism. Soc. Am.* **84,** 91–104.

Zhao, L.-S. and D. V. Helmberger (1996). Regional moments, energy levels, and a new discriminant, *Pure Appl. Geophys.* **146,** 281–304.

Zhu, L. and D. V. Helmberger (1996). Advancement in source estimation techniques using broadband regional seismograms, *Bull. Seism. Soc. Am.* **86,** 1634–1641.

Seismological Laboratory
California Institute of Technology
Pasadena, California 91125

Manuscript received 10 June 1997.